IOP Conf. Series: Materials Science and Engineering **433** (2018) 012075 doi:10.1088/1757-899X/433/1/012075

Enhancement of weld quality of AISI 304L austenitic stainless steel using a direct current pulsed TIG arc

AA Ugla
Department of Mechanical Engineering, College of Engineering, University of Thi-Qar, Al-Nasiriyah-64001, Iraq
E-mail: adnanugla76@gmail.com

Abstract. In welding processes, the quality of weldment usually refers to the desired weld bead geometry and its microstructural characteristics, which affect the mechanical properties of the welded components. The present paper aims to investigate the influences of the main process input factors on weld geometry, metallurgical characteristics, and mechanical properties of weldments of 3.8-mm-thick plates of austenitic stainless steel type 304L using tungsten inert gas welding with pulsed/non-pulsed current processes. This research paper investigates the effects on the arc pressure of pulse frequencies at levels of 6 and 1,000 Hz, and thereby their effects on the aspect ratio and morphology of the weld metal. The key outcomes of this work are that the frequency of arc pulsation has a strong effect on the breaking of the dendritic arms during the welding process. The obtained microstructure results reveal that the structure of the high pulse frequency current welded specimens are thus generally finer grained, with higher levels of residual ferrite and an absence of columnar grains; such pulse frequencies thus strongly influence the tensile strength and microhardness of affected weldments as compared to those seen in continuous current welded specimens. Additionally, the most important factor affecting the bead geometry and aspect ratio is identified as the pulse frequency, with a contribution of 64%.

1. Introduction

Generally, weld quality is significantly affected by the main input parameters. One of the main problems to be faced in terms of the quality assurance of weldments is the control process on the parameters used, as these parameters significantly affect the bead geometry and weld quality, and thus influence welding efficiency. Weld bead geometries affect the weld quality by significantly influencing the mechanical properties [1], and thus the weld quality depends on the weld geometry, metallurgical aspects, and the mechanical properties of the weldments. Bad weld quality may result from coarser grain sizes in the weld metal, larger HAZ, and shallower depth of fusion with higher excess metal, whereas a perfect weld quality may be achieved with adequate depth of penetration, desirable morphological aspects, and suitable weld bead geometry. Gas tungsten arc welding (GTAW) is the most commonly used method for joining stainless steel components, though under the same welding conditions, tungsten inert gas (TIG) welding processes can produce improved mechanical properties as compared to metal inert gas (MIG) welding processes [2]. The technique is particularly suitable for thin sheets since it is easy to use, flexible, and economic [3]. The TIG welding technique can provide good quality weldments of stainless steels [4, 5] and offers superior properties compared to other arc welding techniques [6]. Kumar et al. [7] demonstrated that TIG welding techniques provides greater flexibility to select the most suitable sets of parameters such that the weldments become stronger than the base metal, especially for austenitic stainless steel (ASS). TIG welding performance is generally evaluated on the basis of mechanical properties and aspect ratio; the welded parts are considered good quality when they meet quality requirements such as ultimate

tensile strength (UTS) [8]. Kumar and Sathiya [9] showed that the activated-TIG welding method can be used to improve the performance of traditional TIG techniques. The improvements in weld quality depend on the proper selection of welding parameters, welding methods, and materials used. Pulsed current TIG technique is a variation of the conventional TIG technique, which involves cycling the welding current at a certain pulse frequency [10]. In pulsed current TIG welding (PCTW), the pulsed current (Ip) is usually chosen to melt the filler metal and fuse the base metal to create appropriate depth of penetration, while the base current (Ib) is adjusted to a value capable of keeping the arc ignition and overall process stabile [12]. The PCTW technique is considered a better way to address the aforementioned weld quality problems such as coarse grains at weld and heat affected zones and insufficient depth of penetration. The changes in microstructure and phases of the weld metal depend strongly on the heat input due to different solidification modes [13]. Other studies have investigated the effects of pulsed current on mechanical and metallurgical properties [14-18]. Ugla [11, 19] investigated the effects of pulse frequency and cooling state on the properties of welded joints. He demonstrated that they significantly influence the morphology of the welded parts and hence improve the mechanical properties by significantly affecting the grain size by means of breaking the dendrite arms as well as the making amount of δ-ferrite become relatively higher.

It is important to investigate the possibility of improving weld quality using the PCTW process, and this requires exploration of the characteristics of the arc and molten pool [20]. In the arc welding process, the plasma jet force is considered an important factor affecting the arc pressure (Parc) developed throughout the joining process. It can significantly affect the depth of penetration into the molten pool [21]. The main forces that affect the weld pool overall are gravity, arc pressure, surface tension, and electromagnetic (Lorentz) forces, as shown in figure 1 [22]. Parc in TIG technique is occasioned by impinging the plasma jet onto the weld pool [23].

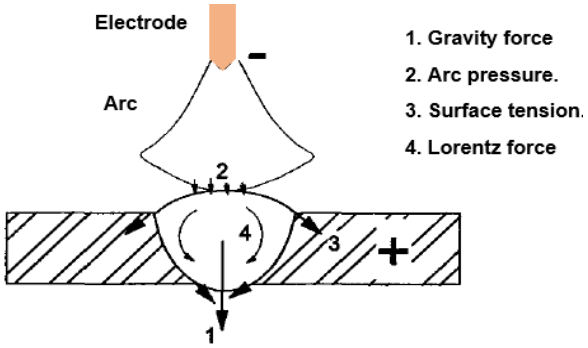

Figure 1. Sketch illustrating the main forces influencing the pool surface

When this arc pressure impacts the liquid metal of the weld pool, it may create flow motion and thus influence the depth of penetration and bead geometry [24]. Radial electromagnetic forces significantly influence on the arc: arc root diameter decreases with increasing frequency [25, 26]. The weld characteristics and fluid flow in the welding pool are thus hugely influenced by arc energy, arc profile, and arc force [27]. Other studies have demonstrated that arc force depends on the square of welding current [23, 28]. However, Ghosh et. al. [29] showed that the arc force is proportional to the pulse frequency. Therefore, Parc can be considered as one of the most important parameters influencing the characterisation of the welded parts. Reported works relevant to the effects of pulse frequency of the arc and pulsed arc pressure on the metallurgical aspects and other properties of the welded parts are scanty, so further investigations are necessary in order to clearly understand the effects of these phenomena. The main aim of the present work is thus to investigate the influences of pulse frequency on the pulsed arc pressure, and thereby to study the effects on the weld quality through an analysis of the aspect ratio of the weld profile, metallurgical aspects, and mechanical characteristics of AISI 304L stainless steel weldments. This research work is an experimental investigation into the effects of arc pulsation on the weld area (HAZ and bead width) and depth of penetration, with the aim of discovering optimal aspect ratios

2. The Materials and experimental procedure

In this work, 3.8 mm thicknesses of similar 304L sheets were welded using the TIG technique. The filler metal selected for welding was ER 308LSi stainless steel solid wire with a diameter of 0.8 mm. The experiments were conducted using a CNC machine, which was used to control the travelling speed of the welding, as shown in figure 2. The suggested shielding gas was Argon at 99.90% purity provided at 12 l/min. The 304L stainless steel plate and the welding metal were chemically analysed, and the results of the analysis are listed in table 1. The plates were cut using a power hacksaw cutting machine. For the bead on plate experiments, the required plate dimensions were 100 mm x 200 mm, whereas for square butt joint configuration, the required plate dimensions were 100 mm x 50 mm. The prepared parts were joined using CCTIG and PCTIG processes by means of a LINCOLN TIG machine, which can be used for both continuous and pulsed currents. The travel speed and arc length were controlled using the CNC machine, whereas the wire feed rate was controlled using an external wire feed machine. The pulsed current mode used in this welding machine is shown in figure 3. AK-Type thermocouple was found to be the most suitable for measuring the welding peak temperature during the welding process [23].

Table 1. The chemical composition of the base and the filler materials (in wt. %)

Element	%C	%Si	%Mn	%S	%P	%Mo	%Ni	%Cr	%Fe	Others
SS304 actual composition	0.015	0.528	1.011	0.011	0.02	0.053	8.20	18.16	Bal.	V = 0.10, Cu = 0.031 Ti =0.01
ER308LSi as deposited composition	0.018	0.56	1.358	0.033	0.033	0.115	9.412	19.56	Bal.	Co=0.941 ; Cu= 0.181 Ti=0.057

Figure 2 Left View of the CNC machine, and right side close-up view of the welding torch and filler wire nozzle

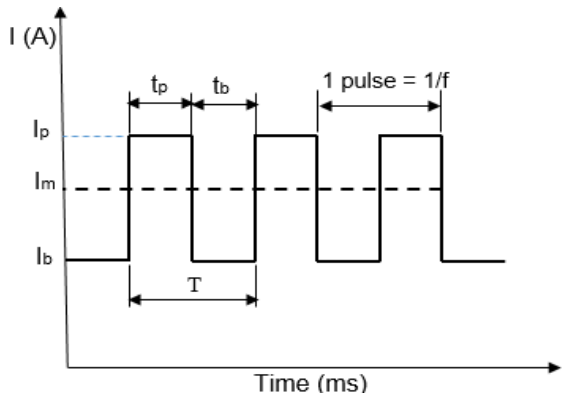

Ip: Pulse current (A)
Ib: base current (5- 95 % of Ip) (A)
Im: mean current = (Ip tp +Ib tb)/ (tp+tb)
tp: peak current duration (ms)
tb: base current duration (ms)
T: cycle time = tp + tb
F: pulse frequency = 1/ T

Figure 3. Schematic diagram of a standard pulse current-time wave form in PC-TW process.

The temperature was read using an industrial data logger, which records the temperature at intervals of one second. In order to reduce the defects in the testing samples, a large number of preliminary trials were carried out using different sets of input parameters. Some of the process parameters were kept constant during all experiments, such as the welding current of 175 A, peak time of 50%, background current of 87.5 A, arc length of 4 mm, wire feed angle of 40°, and stick out of 15 mm.

Thus, in this study, three experimental factors were used to investigate the influence of parameters on weld bead dimensions. The limits of each input parameter were selected based on the preliminary trials. The sets of the selected process parameters used in this work to investigate the effects on the aspect ratio (AR = bead width/depth of penetration) are summarised in table 2. The pulse frequency was set to low frequency (LF) and high frequency (HF). The weld bead profiles of all specimens were measured carefully and the observed values for weld width and depth of fusion were used to calculate the AR and corresponding signal/noise (S/N) ratios, as summarised in table 2. Based on the performance characteristics, three S/N values were available, namely the higher the better, the lower the better, and nominally the better. In the current work, the aspect ratio (W/P) was identified as the response. Depth of penetration was considered to be the required sign and the bead width of the tested welding specimens was considered to be an undesirable sign. Therefore, the aspect ratio was considered under smaller the better (SB) conditions to minimise the aspect ratio of the welded parts. The smaller the better performance is expressed as

$$S/NSB = -10 \log \{(y12 + y22 + y32 \ldots yn2)/n\} \quad (1)$$

where y is the response and n is the number of repetitions of output response in the same trial.

Table 2. Welding conditions for preparing tests specimens of butt joint weldments and responses

Exp No.	Welding process	Input factors			Response signs		
		Travel speed TS (mm/s)	Wire feed speed WFS (m/min)	Frequency F (Hz)	Aspect ratio (W/P)	S/N ratio	Peak temperature °C
1	CC TW	1	0	0	4.47	-13.013	1046.45
2		2	4	0	3.8157	-11.631	1040
3	PCTW LF	1	2	6	3.6842	-11.327	996.9
4		3	4	6	3.3333	-10.457	1020
5	PCTW HF	1	4	1000	3.3157	-10.411	978
6		2	2	1000	2.6	-8.317	990.5

The microstructure evolutions in the CCTW and PCTW processes were extensively investigated in this study to develop understanding of the influences of the arc pulsation on the surface morphology and microstructure characteristics of the weldments. Optical microscopy was used to obtain microphotographs, and cross-section specimens were prepared for metallographic tests using the standard procedures reported in the literature [30]. All specimens were electro-etched using 10 g oxalic acid in 100 ml distilled water at 9 V for 30 to 60 secs.

Transverse tensile tests were done on subsize sheet specimens with a 25 mm gauge length, and 6.25 x 3.8 mm2 cross-sections were prepared based on ASTM: E8/8M standards [31], as shown in figure 4. Each value reported is the average of three tested specimens.

Microhardness testing was done to determine the hardness value of the centre of the weld metal for the PCTW specimens and to compare the results with the CCTW specimens. The microhardness measurements were taken at the centre of the weld metal using a Vickers' tester with a test load of 300 g for a dwell period of 15 secs and interval of 0.5 mm.

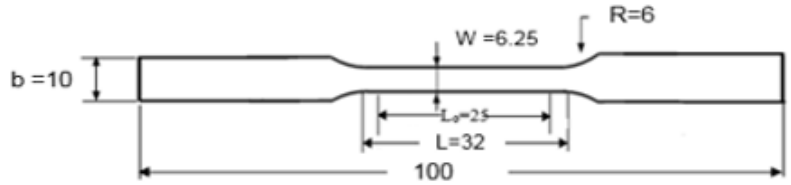

Figure 4. Schematic illustrating sub-size standard tensile specimen prepared according to ASTM E8/8M [30].

3. Results and discussions

Generally, the HAZ decreased the ultimate strength of the welded parts and reduced the efficiency of the joints due to metallurgical changes at this region such as grain growth. Most of the tensile test specimens failed at HAZ. Thus, the HAZ should be reduced to a minimum by reducing the heat input, shortening the cooling time, and using a pulsed current welding method with high frequency. The higher the pulse frequency (F), the more obvious arc shrinkage; the root radius of the arc reduces with increasing F, as shown in figure 5(b). This result is consistent with the findings of Qi and others [27].

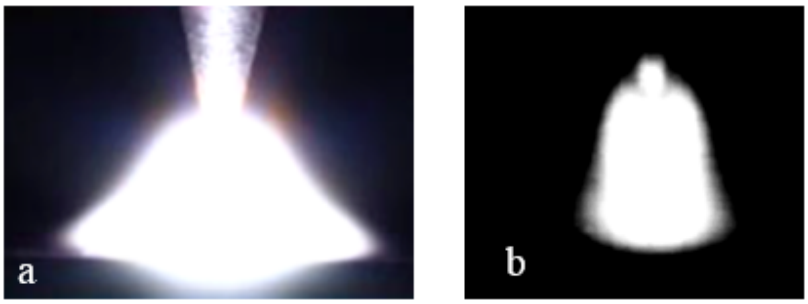

Figure 5. TIG phenomena obtained at (a) 0 Hz CCTW and (b) 1000 Hz PCTW. Both arc welds were produced with a 3.2 mm tungsten electrode

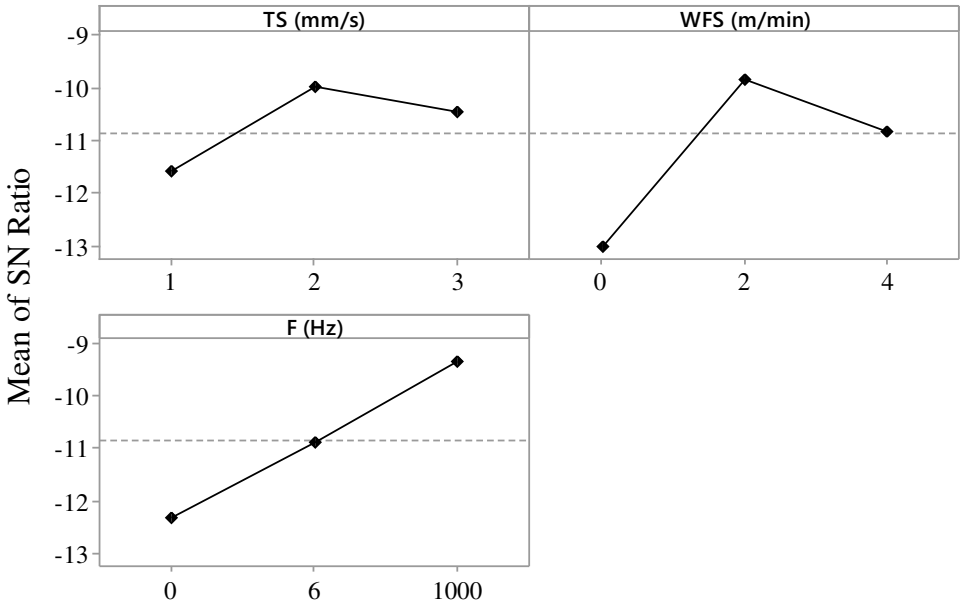

Figure 6. Plots illustrating the effects of main factors on S/N ratios of the aspect ratio of weld bead geometry.

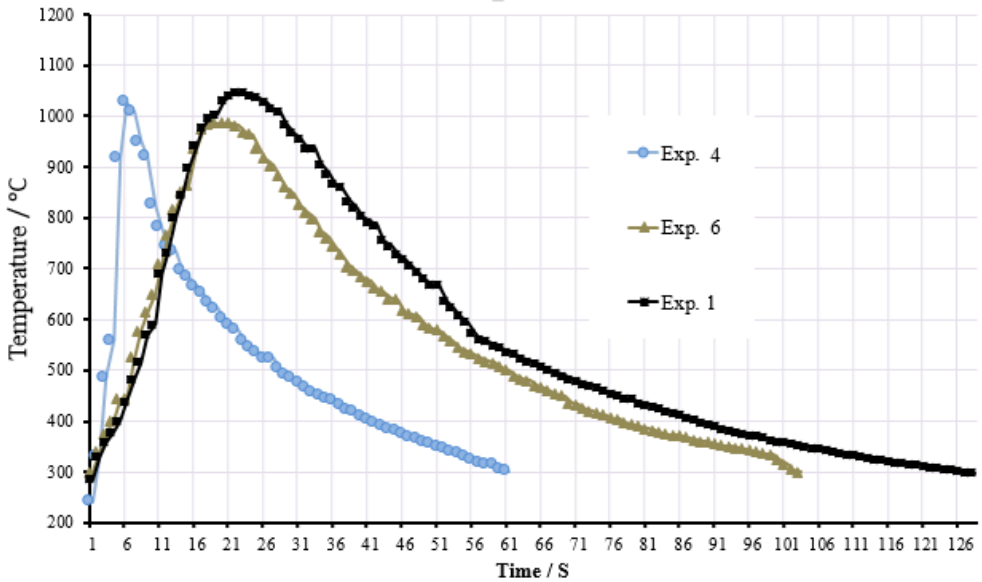

Figure 7. Plots illustrating heating and cooling curves

Table 3. Optimized parameters for lower aspect ratios (AR)

S. No	Factor	Level	Value	Rank	Percent contribution
1	TS	2	2 mm/s	2	16.2 %
2	WFS	2	2 m/min	3	2.91 %
3	F	3	1000 Hz	1	63.75 %

The various aspect ratios of bead width and depth of penetration were calculated experimentally for all experiments as listed in table 2. Figure 6 shows the plots of the S/N ratios, and it is obvious that the S/N values increase with increases in the pulse frequency, as well as with the increase in TS from 1 mm/s to 2 mm/s and the increase in WFS from 0 m/min to 2 m/min. However, a decrease is observed when increasing the WFS from 2 m/min to 4 m/min, and on increasing the TS from 2 mm/s to 3 mm/s. It is obvious that with high frequency (exp. 5 and exp. 6), the welded area significantly reduces; the arc was more restricted and the temperature concentrated, improving the weldment quality. The welded area of the conventional welding process was relatively larger, which may be attributed to the fact that in the CCTW process, the arc diameter is larger (see figure 5(a)), and this increases the exposure area to high temperature leading to an increase in the HAZ zone.

Analysis of figure 6 sugests that the optimal parameters can be identified as listed in table 3. A travel speed of 2 mm/s, filler wire at 2 m/min, and a frequency of 1,000 Hz gave the optimum aspect ratio when using the welding conditions reported in table 2 for preparing welded specimens of similar AISI 304L plates. The heating and cooling curves for CCTW (experiment 1), low-frequency PCTW (experiment 4), and high-frequency PCTW (experiment 6) are shown in figure 7. The values of peak temperature are summarised in table 2. The peak temperature of the HF-PCTW process was less than those of the LF-PCTW and CCTW processes. This can be attributed to the influence of high frequency on the arc radius, whereby heat is focused within the HF-PCTW process and the thermocouple read a lower temperature than in the CCTW process. Figure 8(a)-(b) shows the weld bead profiles of experiments 1, 4, and 6 which represent the CCTW, LF-PCTW, and HF-PCTW processes. It is obvious that the bead width of the CCTW process is larger than that of the PCTW. This means that the HF-PCTW gives most suitable aspect ratio because of its high penetration and low bead width; hence, an optimal aspect ratio can be achieved in this process.

From the microstructure results, it is clear that two different kinds of δ-ferrite, lathy and skeletal δ-ferrite, are formed in the austenitic matrix. Figure 9 compares the parent metal, HAZ, fusion zone, and metal at welding center of CCTW, LF-PCTW, and HF-PCTW weldments. It can be seen that the microstructure of all welding processes includes columnar dendritic arms and that these grow in the steepest cooling rate direction. It is obvious that the heat affected area in PCTW process is narrower than that of the CCTW process. This can be attributed to the effect of arc radius (see figure 5) and also to the lowered heat input in the PCTW process as compared to the CCTW process. The grains in HAZ near fusion boundary are coarse, and for CCTW weldments, the low cooling rate leads to grain growth at the HAZ (figure 9), whereas for the PCTW weldment, the pulse frequency has a significant effect on the solidified weld pool and thus results in less grain growth. The grain structures in the center of the weld metal (WM) for CCTW, LF-PCTW, and HF-PCTW are shown in figure 10. The microstructures in figure 9 reveal that HF-PCTW process causes the creation of a smaller grain structure with an absence of columnar dendritic arms throughout the microstructure. This can be attributed to effects of the pulse frequency.

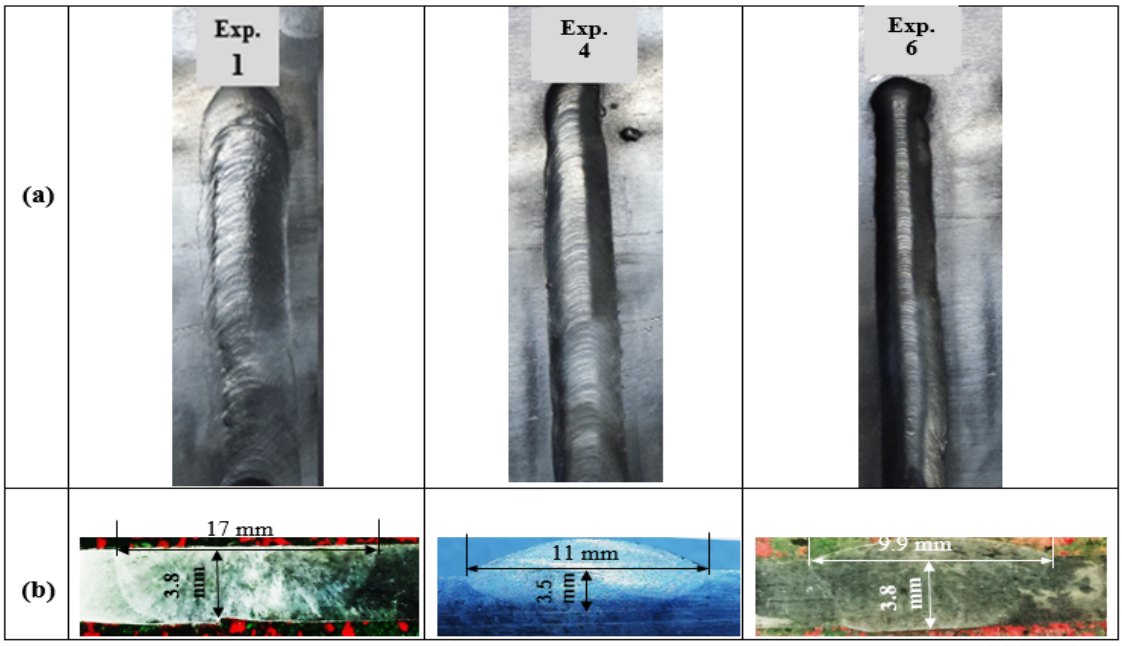

Figure 8. Optical macrophotographs of experiments 1, 4, and 6 showing (a) weld bead profiles; (b) cross-section profiles

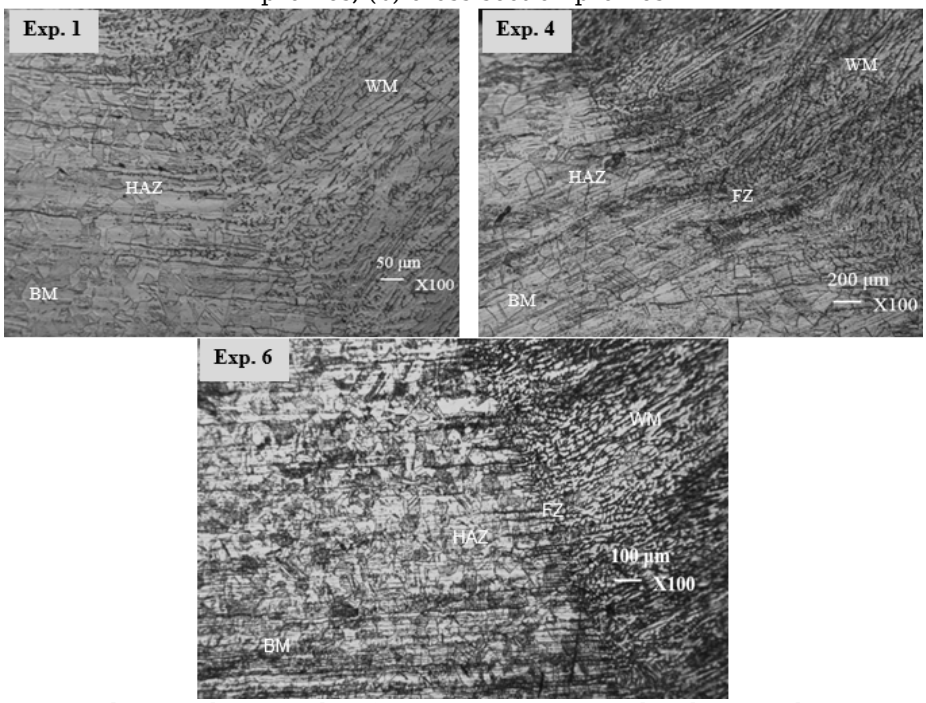

Figure 9. Optical microphotographs of experiments 1, 4, and 6 showing the microstructure of the base metal (BM), HAZ, fusion zone (FZ), and weld metal

The changes in microstructure associated with the amount of heat input to the weld pool during the deposition process emerge according to Eq. (2) [15].

$$\mathrm{Hi}\left(\frac{\mathrm{J}}{\mathrm{mm}}\right) = \eta \mathrm{I} \frac{\mathrm{V_{av}}}{\mathrm{TS}} \qquad (2)$$

where Hi refers to heat input per unit distance, η is arc efficiency (assumed to be 0.83 for TIG welding) [16], and Vav is the average of the instantaneous arc voltage (15 volts).
In the PCSMD process, the heat input can also be calculated using Eq. (2), but here the

welding current is Im, as shown in Eq. (3) [32, 33].

$$\mathrm{Hi}\left(\frac{\mathrm{J}}{\mathrm{mm}}\right) = \eta\, \mathrm{I_m}\, \frac{\mathrm{V_{av}}}{\mathrm{TS}} \qquad (3)$$

Thus, the heat input in CCTW is about 1,039 J/mm, whereas the Hi for the PCTW process is about 817 J/mm. The amount of δ-ferrite existing in the weld metal depends on the significant parameters such as the chemical composition of the used materials, welding procedure, and amount of heat input to the melting pool during the welding process [34]. Furthermore, the process of rapid solidification with a high temperature gradient is beneficial to obtain a finer microstructure. Low heat input to the weld zone may result from high travel speed, or the use of high pulse frequencies. Figure 10 reveals a higher residual ferrite amount in the HF-PCTW process, which can be attributed to the high cooling rates associated with arc pulsation or high travel speed; the high cooling rate leads to suppression of the transformation of δ-ferrite to austenite. High frequency also leads to breaking of the dendritic arms of austenitic stainless steels and produces a more uniform structure. Figure 9 describes the effects of high-frequency (1,000 Hz) pulsed current on columnar grains as compared to conventional current processes.

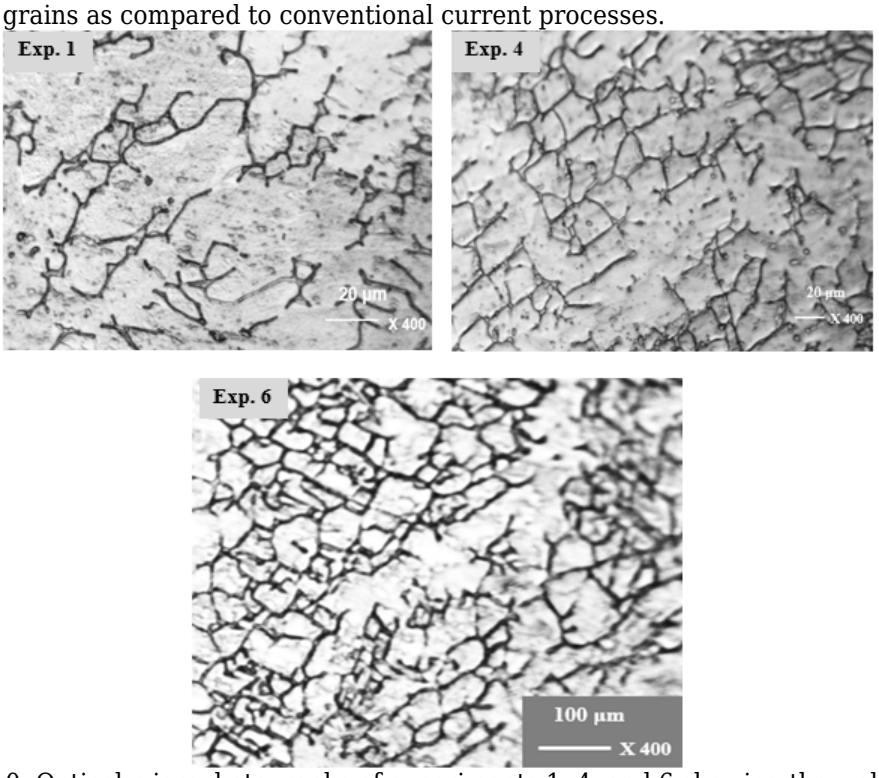

Figure 10. Optical microphotographs of experiments 1, 4, and 6 showing the weld metal.

It is obvious that the pulse frequency significantly affects the dendrite arms of the solidified structure at the weld metal; hence, it influences the tensile properties of welded parts. This can be attributed to the strong correlation of the Parc (arc force) and arc pulsation. The relationship between Parc, welding current, and arc diameter was derived by Lin and Eagar, as expressed in Eq.(4) [23]:

$$\mathrm{Parc} = \frac{\mu_o \mathrm{I}^2}{4\,\pi^2\,\mathrm{R}^2} \qquad (4)$$

where μ_o is the magnetic permeability of free space, R is the Arc radius, and I is the Welding current.

In the PCTW process, the average of pulsed current can be calculated using Eq. (5) [35]:

$$\mathrm{I_m(A)} = \frac{\mathrm{I_p\, t_p + I_b\, t_b}}{\mathrm{t_p + t_b}} \qquad (5)$$

where Im, tp, tb, Ip, Ib are as defined in figure 2.

Alongside the four pulsing parameters, Ip, Ib, tp, and tb, the pulsing frequency is used as

an operational parameter in terms of total cycle time, as shown in equation (6) and as described in figure 2.

$$F\,(Hz) = \frac{1}{t_p + t_b} \qquad (6)$$

Substituting (5) and (6) into (5) yields the pulse arc pressure as per Eq.(7)

$$P_{arc}(Pa) = \frac{\mu_o}{4\,\pi^2 R^2} F^2\, I_b^2 \left(C\,t_p + t_b\right)^2 \qquad (7)$$

where Ib is background current, and C is the current ratio (C = Ip/Ib)

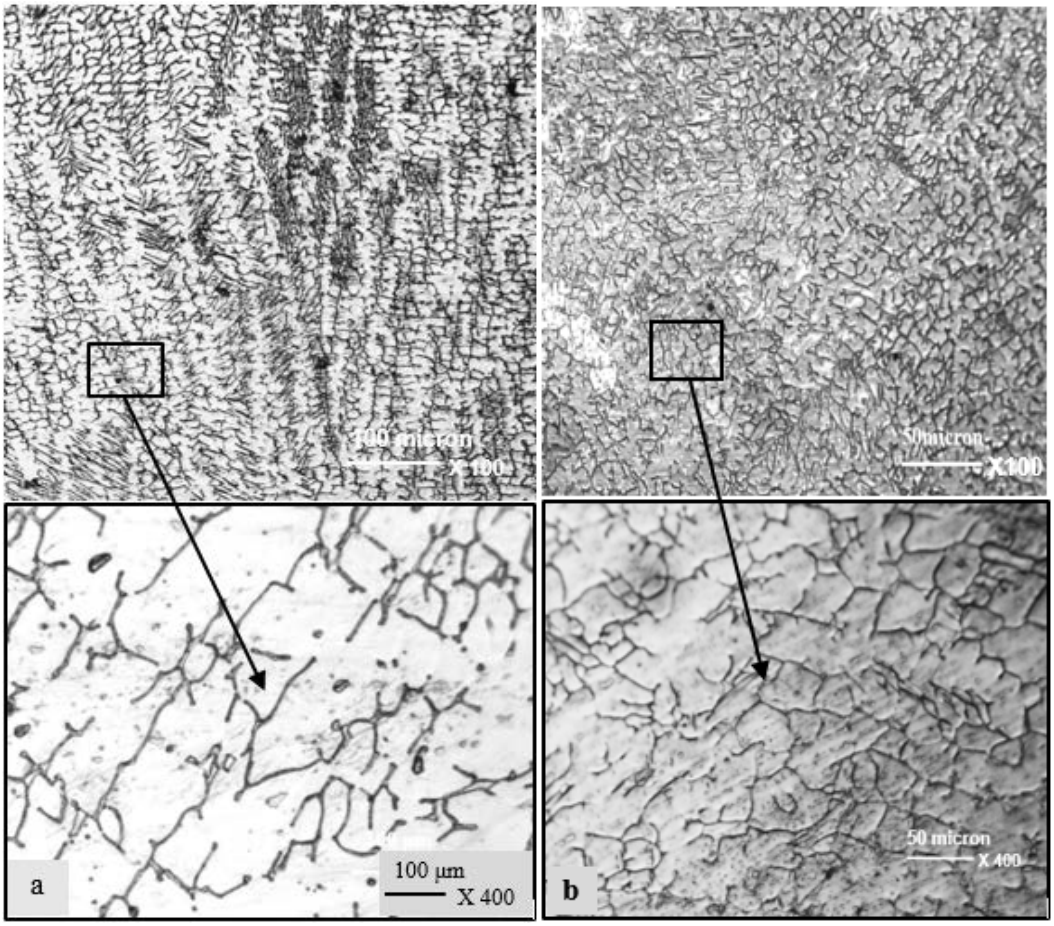

Figure 11. Micrographs illustrating the effects of frequency on dendritic arms (a) continuous current (exp. 1) and (b) HF pulsed current (exp. 6), showing the microstructure texture of CCTW and HF-PCTW

Eq. (7) shows that Parc is correlated to the pulse frequency, arc diameter, and the current ratio. In this study, the current ratio was kept constant (C = 2) and the arc radius reduced with increasing pulse frequency (see Fig. 4); therefore, the arc pressure (arc force) significantly increased with increases in the pulse frequency [22, 26], which offers a reasonable explanation for the microstructure changes with changes in frequency seen in figure 10(b). Eq.(7) also shows that the Parc does not depend o other process parameters such as travel speed and wire feed rate [36]. Figure 11(a) shows that AISI304L stainless steel weldments solidify by means of dendritic growth. The pulse arc pressure produces oscillation that breaks these dendritic arms and creates additional nucleation sites, hence causing refinement of the structure (see Figs. 10 and 11(a)).

The tensile stress-strain curves for the CCTW, LF-PCTW, and HF-PCTW welded specimens are shown in Fig. 12. The highest tensile strength and largest elongation were achieved in the HF-PCTW process.

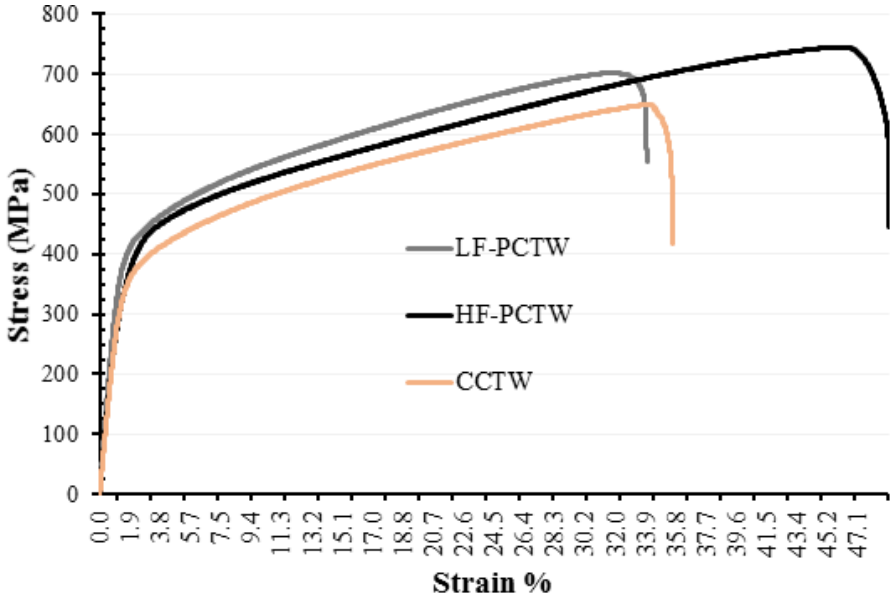

Figure 12. Plot showing the tensile stress-strain curves for CCTW, LF-PCTW, and HL-PCTW specimens

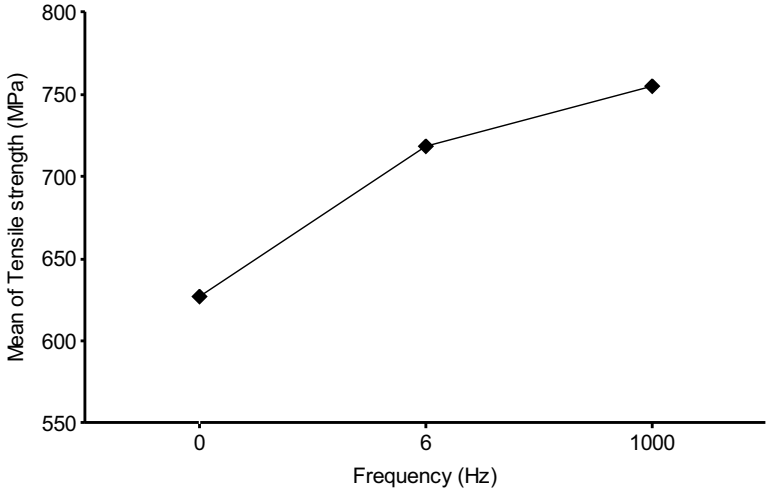

Figure 13. Plot illustrating ultimate tensile strength versus F.

The relationship between ultimate tensile strength and pulse frequency can be seen clearly in figure 13. It is obvious that the highest ultimate strength was achieved at the highest frequency (1,000 Hz), followed by that seen using the low frequency (6 Hz). The highest tensile strength achieved during this research was 765.8 MPa at a frequency of 1,000 Hz; the tensile strength obtained in the standard CCTW process was 671.73 MPa. Figures 12 and 13 indicate that the welding procedure adopted in this work using the HF-PCTW welding process was capable of providing tensile properties superior to those of CCTW and LF-PCTW, but comparable to the base metal; some specimens even gave slightly higher results than the base metal.

Figure 14 shows the significant effects of frequency on micro-hardness by significantly affecting the grain size by breaking dendrite arms as well as causing the amount of δ-ferrite to be relatively higher (Fig. 11(b)). Figure 15 shows the Vicker's microhardness (HV) profiles across CCTW, LF-PCTW, and HF-PCTW weldments. It is obvious that the hardness distribution is highest in the weld metal center (WM) for all weldments, whereas the HAZ hardness is reduced for all weldments due to the relatively large grain size with increased

distance from the weld center. As can be seen in the Fig. 14, the hardness of the HF-PCTW joint is the highest as compared to LF-PCTW and CCTW joints. This phenomenon can be attributed to pulse frequency affects on the residual delta-ferrite (δ-ferrite) content as well as the grain refinement in the weld zone. Furthermore, high pulse frequency leads to increase pulsed arc pressure (Eq. 7) and hence leads to blocking and breaking columnar grains. The hardness variation thus not only depends on the degree of grain refinement but also on phase formation [37]. The higher residual δ-ferrite and finer grain structure usually leads to increased hardness of the weldments of the HF-PCTW (see figure 14). On the another hand, the high frequency leads to a reduction in the HAZ zone, attributable to the fact that the arc radius significantly reduces with increased pulse frequency (see figure 5). The hardness of the HAZ zone in HF-PCTW weldment is relatively larger than in other forms due to the small grain size (see exp. 6 in figure 9). Thus, the frequency can be considered as the most important factor influencing weld metal microhardness. The highest Vicker's microhardness numbers (VHN) of the obtained microhardness in the weld metal zones are 308 VHN for the HF-PCTW, 292 VHN for the LF-PCTW, and 262 VHN for the CCTW.

The mechanical testing (tensile and microhardness tests) of properties indicated that there was a strong correlation between the arc pressure and pulse frequency; this leads to increases in the grain refinement and also increases the residual δ-ferrite amount. The pulse frequency thus affects the weld microstructure,which in turn influences the weld hardness and tensile strength.

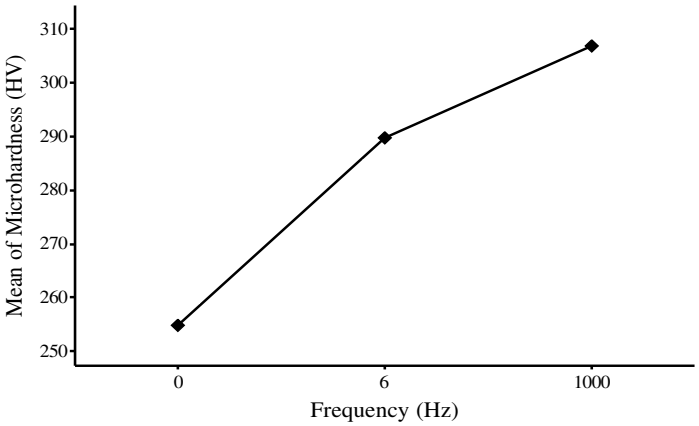

Figure 14. Plot showing the effects of pulse frequency on microhardness (HV).

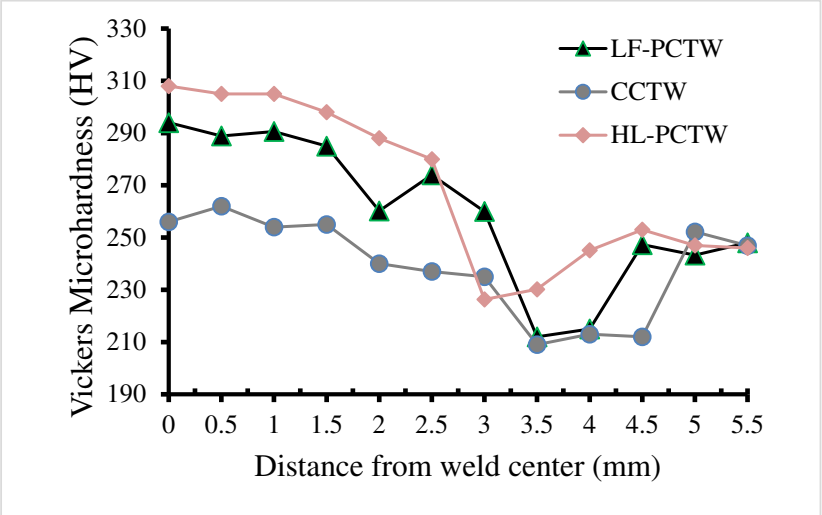

Figure 15. Microhardness (HV) across welding cross-sections for CCTW, LF-PCT, and HF-PCTW weldments.

4 Conclusions

This paper investigated the improvement of weld quality by means of experimental study selecting and controlling process parameters using 3.8 mm sheets of AISI 304L stainless steel material welded using both non-pulsed and pulsed current TIG welding. The main findings of this study can be summarised in the following conclusions:

1. The pulse frequency is the most important parameter influencing the aspect ratio, with a contribution percentage of 64%; other parameters make much smaller percentage contributions.
2. Optimal aspect ratio can be achieved by using the HF-PCTW process with the following optimal values of welding conditions: F=1000 Hz, TS=2 mm/s, and WFS=2 m/min. High pulse frequency strongly improved the quality of AISI 304L welded parts by significantly reducing the HAZ and increasing the depth of penetration.
3. In the HF-PCTW process, the arc energy concentrates at a shrinking arc radius, which leads to an increase in the depth of penetration and also increases the pulsed arc pressure. The pulsed arc pressure is the main reason for the significant changes in the weld metal grain size and texture.
4. From the morphology of the welded parts, in both processes, the structure is mainly composed of primary ferrite (lathy/vermicular) and austenite. PCTW components reveal microstructures with relatively fine grains and high residual ferrite contents compared to CCSMD specimens.
5. The highest tensile strength achieved in this study was 766 MPa using a frequency of 1,000 Hz. This was comparable to the base metal and superior to the conventional process. This can be attributed to the important changes in the morphology associated with pulse frequency.
6. The resulting microstructure consisted of relatively small grains with high amount of residual ferrite in case of the HF-PCTW process. This is the main cause of increased micro-hardness in the weld zone, whixch reached 308 in comparison to the CCTW process, which reached 262.

References

[1] Benyounis KY and Olabi AG 2008 Optimization of different welding processes using statistical and numerical approaches- *A reference guide Advances in Engineering Software* **39** pp 483-96.

[2] Satheesh Kumar KV, Gejendhiran S and Prasath M 2014 Comparative investigation of mechanical properties in GMAW/GTAW for various gas compositions *Mater. Manuf. Proc.* **29** pp 996-1003.

[3] Mao J, LÜ W, Wang L, Zhang D and Qin J 2014 Microstructure and mechanical properties of GTA weldments of titanium matrix composites prepared with or without current pulsing *Transaction of Nonferrous Metals Society of China* **24** pp 1393-99

[4] Fujii H, Sato T, Lu SP, and Nogi K 2008 Development of an advanced A-TIG (AA-TIG) welding method by control of Marangoni convection Mater. *Sci. Engi. A* **495** pp 296–03

[5] Ganesh KC, Vasudevan M, Balasubramanian KR, Chandrasekhar N, and Vasantharaja P 2014 Thermo-mechanical analysis of TIG welding of AISI 316LN stainless steel *Mater. Manuf. Proc.* **29** pp 903-09

[6] Pramanik A, Littlefair G, and Basak A K 2015 Weldability of duplex stainless steel *Mater. Manuf. Proc.* pp 01-16

[7] Kumar S A, and Sathiya P 2015 Experimental Investigation of the A-TIG welding process of Incoloy 800H *Mater. Manuf. Proc.* pp 01-6

[8] Kumar K, and Sundarrajan S 2009 Optimization of pulsed TIG welding process parameters on mechanical properties of AA5456 aluminum alloy weldments *Mater. Des.* **3** pp 1288-97

[9] Kumar S, and Shahi A S 2014 On the influence of welding stainless steel on microstructural development and mechanical performance Mater. Manuf. Proc. 29 894-02. Doi: 10.1080/10426914.2013.792421.

[10] Tathgir S, Bhattacharya A, and Bera TK 2014 Influence of current and shielding gas in TiO2 flux activated TIG welding on different graded steels Materials and Manufacturing Processes

[11] Ugla AA 2016 A comparative study of pulsed and non-pulsed current on the aspect ratio of weld bead and microstructure characteristics of AISI 304L stainless steel *Innovative System Design and Engineering* **7** pp 88-98.

[12] Yousefieh M, Shamanian M, and Saatchi A 2011 Optimization of the pulsed current gas tungsten arc welding (PCGTAW) parameters for corrosion resistance of super duplex stainless steel (UNSS322760) welds using the Taguchi method *Alloys and Compounds* **209** pp 782-90

[13] Murti VSR, Srinivas PD, Banadeki GHD, and Raju KS 1993 Effect of heat input on the metallurgical properties of HSLA steel in multi-pass MIG welding *Mater. Proc. Technol.* **37** pp 723–29.

[14] Shengsun H Ruifeng H, Junqi S, Jian H, and Haigang X 2013 Effect of pulse frequency on microstructure of 21%Cr ferritic stainless steel in pulsed gas tungsten arc welding Transactions of Tianjin University **19** pp 127-29

[15] Yang M, Qi B, Cong B, Liu F, and Yang Z 2013 Effect of pulse frequency on microstructure and properties of Ti6Al4V by ultrahigh-frequency pulse arc welding *Int. J. Adv. Manuf. Technol.* **68** pp 19-31

[16] Gridharan PK and Murugan N 2009 Optimization of pulsed GTA welding process parameters for the welding of AISI 304L stainless steel sheets *Int. J. Adv. Manuf. Technol*. **40** pp 78-89

[17] Karunakaran N 2012 Effect of pulsed current on temperature distribution, weld bead profile and characteristics of GTAwelding stainless steel joints *Int. J. Eng. Technol*. **2** pp08-16.

[18] Ramkumar KD, Choudhary A, Aggarwal S, Srivastava A, Mohan TH, and Arivazhagan N 2015 Characterization of microstructure and mechanical properties of continuous and pulsed current gas tungsten arc welded super austenitic stainless steel *J. Mat. Res.* **30** pp 1727-46.

[19] Ugla AA 2016 Characterization of Metallurgical and Mechanical Properties of the Welded AISI 304L Using Pulsed and Non-Pulsed Current TIG Welding International Science Index *Materials and Metallurgical Engineering* **10** pp 463-70.

[20] Ham HS, Oh DS and Cho SM 2012 Measurement of arc pressure and shield gas pressure effect on surface of molten pool in TIG welding *Science and Technology of Welding & Joining* **38** p 594

[21] Yang M, Yang Z and Qi B 2015 The effect of pulsed frequency on the plasma jet force with ultra-high-frequency pulsed arc welding *Weld World* **59** pp 875–882

[22] Kou S 2003 Welding Metallurgy 2nd Edition *John Wiley &SONS, INC*. pp 97-115

[23] Lin ML and Eagar TW 1986 Pressure produced by gas tungsten arcs *Metallurgical Transaction* **178** pp 601-07.

[24] Yamauchi N and Taka T 1979 TIG arc welding with a hollow tungsten electrode *International Institute of Welding document* no.: 212-452-79.

[25] Zhao JR, Sun D, and Hu SS 1992 Arc behavior of high frequency pulse TIG welding arc Transactions of the *China Welding Institute* **13** pp 59–66.

[26] Chen SJ, Zhang BL, Yin SY and Wu HR 2006 Effects on aluminumalloy TIG welding quality of double pulse modulated variable polarity waveform *Electric Welding Machine* **36** pp 7–14

[27] Qi BJ, Yang MX, Cong BQ, Liu FJ 2013 The effect of arc behavior on weld geometry by high-frequency pulse GTAW process with 0Cr18Ni9Ti stainless steel *Int. J. Adv. Manuf. Technol.* **66** pp 1545–53

[28] Cook GE, El-deam H and Eassa EH 1985 The effect of high frequency pulsing of a welding arc *IEEE Transactions on Industry Applications 1A* **21** pp 1294–99

[29] Ghosh PK, Dorn L, Hübner M and Goyal VK 2007 Arc characteristics and behavior of metal transfer in pulsed current GMA welding of aluminum alloy *J. Mater. Proc. Technol.* **194** pp 163–75.

[30] Metals Handbook, Metallographic, structures and phase diagrams. 8th Edition, *American Society for Metals* Metal Park, Ohio 44073 USA 1973.

[31] ASTM International 2011 Standard test methods for tension testing of metallic materials (metric). Standard E8/E8M-09 *ASTM International* W. Conshohocken, Pa

[32] Griridharan PK, and Murugan N 2009 Optimization of pulsed GTA welding process parameters for the welding of AISI 304Lstainless steel sheets *Int. J. Adv. Manuf. Technol.* **40** pp 478-89

[33] Arivarasu M, Devendranath K and Ramkumar Arivazhagan N 2014 Comparative studies of high and low frequency pulsing on the aspect ratio of weld bead in gas tungsten arc welded AISI 304L plates *Procedia Engineering* **97** pp 871-80

[34] Eghlimi A, Shamanian M and Raeissi K 2013 Dilution and ferrite number prediction in pulsed current cladding of super-duplex stainless steel using RSM *Materials Engineering and Performance* **22** pp 3657-64

[35] Farahani E, Shamanian M, and Ashrafizadeh F 2012 A comparative study on direct and pulsed current gas tungsten arc welding of alloy 617 *International Journal on Manufacturing and Material Science* **2** pp 1-6

[36] Savage WF, Nippes EF, and Agua K 1979 Effect of Arc Force on Defect Formation in GTA Welding *Welding Research Supplement* pp 212-24

[37] Ghosh PK, Gupta SR and Randhawa HS 2000 Characteristics of a Pulsed-Current, Vertical-Up Gas Metal Arc *Weld in Steel Metallurgical and Materials Transactions* **31A** 2247–59